JOURNAL OF MATERIALS SCIENCE 23 (1988) 1660–1672

Chemical constitution and microstructure of TiC_x coatings chemically vapour deposited on Fe–C substrates; effects of iron and chromium

W. G. SLOOF, R. DELHEZ, Th. H. de KEIJSER, D. SCHALKOORD
Delft University of Technology, Laboratory of Metallurgy, Rotterdamseweg 137, 2628 AL Delft, The Netherlands

P. P. J. RAMAEKERS
Centre for Technical Ceramics TNO-TUE (C.T.K.), P.O. Box 513, 5600 MB Eindhoven, The Netherlands

G. F. BASTIN
Laboratory of Physical Chemistry, C.T.K., Eindhoven University of Technology, P.O. Box 513, 5600 MB Eindhoven, The Netherlands

TiC_x coatings were chemically vapour deposited in an industrial reactor on Fe–C substrates with carbon contents between 0.06 and 1.20 wt% C. Electron probe microanalyses showed that significant amounts of chromium and iron were present in the coatings and that chromium was also present in the substrate region adjacent to the coatings. By comparing calculated and measured lattice parameters (corrected for the internal stresses present) it became evident that the chromium was in solid solution in TiC_x, whereas the iron was not. This was confirmed by micro Auger electron spectroscopy and X-ray diffraction phase analyses. The carbon to metal ratio, x, of the TiC_x coatings decreased with increasing distance to the coating/substrate interface. The effect of iron on the X-ray diffraction line broadening and hardness of the coatings was large (in contrast with the effect of chromium) and increased with increasing distance to the coating/substrate interface because of a decreasing iron particle size. The TiC_x crystallite size was small and constant throughout the thickness of the coatings. The chromium present in the substrate region adjacent to the TiC_x coatings influenced the microstructure of the substrate by formation of iron, chromium-carbides and reduced the growth rate of the coatings.

1. Introduction

Chemically vapour deposited (CVD) TiC_x coatings are well known for their wear and corrosion resistance [1]. For example, the lifetime of steel cutting and forming tools increases by one to two orders of magnitude if they are coated with TiC_x.

Many characteristics of TiC_x (e.g. hardness [2–5], carbon diffusivity [6, 7], electrical resistivity [8]) depend on its carbon content x which can vary between 0.61 and 0.96 [9]. Therefore knowledge of the composition of TiC_x is important for understanding the relations between properties and deposition circumstances.

It is not generally realized that elements such as oxygen, chlorine, chromium and iron are usually present in TiC_x coatings chemically vapour deposited in an industrial reactor system, and that these may influence coating properties. In the present investigation the chemical constitution and microstructure of such TiC_x coatings on Fe–C substrates are studied. Electron probe microanalysis (EPMA), micro Auger electron spectroscopy (AES), X-ray diffractometry (XRD), light microscopy and microhardness measurements were employed.

The method of determination of solid solubilities from lattice parameters is well known. A complication exists for the TiC_x coatings investigated: both long-range stresses and elements such as oxygen, chlorine, chromium and iron may change the value of the lattice parameter. This complication is dealt with in this paper. For a report of the internal stresses in the specimens investigated, the reader is referred to Sloof *et al.* [10].

It will be shown that the chemical constitution and the microstructure of the TiC_x coatings are closely related.

2. Specimen preparation

2.1. Fe–C substrates

Fe–C substrates were used with carbon contents varying between 0.06 and 1.20 wt % C. The carbon contents were determined by combustion analysis (see Table I). The substrates were prepared from very pure powders of iron (99.999 wt %, Ventron, FRG) and carbon (99.5 wt %, Ventron, FRG) in the following way. An alumina container with iron powder (previously reduced in hydrogen at about 1100 K) was evacuated to 10^{-2} Pa. Then the iron was melted in a pure argon

0022–2461/88 $03.00 + .12

TABLE I Composition at the free surface of CVD TiC_x coatings on Fe–C substrates: series A, B and C. Analyses by EPMA

Substrate C content (wt %)	Coatings								
	C content			Cr content			Fe content		
	A (at. %)	B (at. %)	C (at. %)	A (at. %)	B (at. %)	C (at. %)	A (at. %)	B (at. %)	C (at. %)
0.27 ± 0.01	45.7	45.8	45.7	2.5	1.3	0.7	1.0	1.2	0.8
0.48 ± 0.02	46.0	46.0	–	3.2	1.9	–	1.0	1.0	–
0.76 ± 0.04	46.4	46.2	47.5	3.0	1.9	1.2	1.2	1.3	1.2
0.93 ± 0.05	46.5	46.6	47.3	3.0	2.0	1.3	1.2	1.2	1.2
1.20 ± 0.06	46.4	46.7	47.8	3.2	2.0	1.3	1.4	1.3	1.4
Error:		±0.3			±0.1			±0.1	

Coatings on Fe + 0.06 wt % C were too thin for accurate analyses.
Oxygen and chlorine content of coatings ≤ 0.5 at. %.

atmosphere (using high-frequency induction heating). A calculated quantity of carbon powder was then added and dissolved in the iron melt. Several evacuation, solidification and remelting steps were used to ensure that a homogeneous and pure Fe–C alloy was formed, without gas inclusions. The melt was poured into a cylindrical graphite mould (diameter 30 mm) for the final solidification. The total aluminium content of the substrates after this preparation was found to be about 4×10^{-3} wt %.

After solidication, the Fe–C rods were sawn into slices of about 10 mm thickness using a diamond saw. Both sides of all substrates were mechanically polished (final stage 1 μm diamond), ultrasonically cleaned in ethanol, degreased with freon and slightly etched in a 2% nital solution prior to coating with TiC_x.

2.2. The CVD process

The CVD process was carried out in a standard industrial reactor system (Bernex Co., Switzerland) with a reactor vessel of stainless steel (iron with 24 to 26 wt % Cr, 19 to 23 wt % Ni, 0 to 3.5 wt % C). In the first run, TiC_x was deposited on the substrates over 5 h at 1273 ± 5 K from hydrogen gas (99.998 vol %, Philips, The Netherlands) with 3 vol % $TiCl_4$ (> 99 vol %, Merck, The Netherlands), at a total pressure of 6.7 kPa and a gasflow of 4 l min^{-1} (specimen series A). In two additional runs (specimen series B and C) the substrates were coated under the same conditions but with 3 vol % CH_4 (99.95 vol.%, Air Products, The Netherlands) added to the gas atmosphere. In specimen series B and C not only carbon from the substrate, but also carbon from the gas atmosphere contributed to TiC_x formation. After layer deposition the specimens were allowed to cool in the reactor in a protective hydrogen atmosphere; this took about 2 h.

2.3. Samples for analyses

For the investigation of cross-sections two pieces of about 5 mm × 5 mm and 2 mm thick were cut with a diamond saw from the TiC_x/Fe–C specimens. In order to avoid curvature of the edges of the TiC_x coatings during grinding and polishing, the two pieces were mounted in a steel holder with the TiC_x coatings towards each other and an aluminium foil in between. First the assembly was ground with SiC emery paper (final stage 14 μm SiC) and then lapped with 9 μm diamond followed by mechanical polishing (final stage 1/4 μm diamond). After each preparation step the assembly was ultrasonically cleaned in ethanol. After the final diamond polish an etching in a 2% nital solution was applied.

For EPMA at the free surface of the TiC_x coatings, a piece of about 5 mm × 5 mm and 5 mm thick was cut with a diamond saw from the TiC_x/Fe–C specimens. These samples were moulded in a conductive mounting compound (Resin-2, Struers, Denmark). Surface roughness was removed by grinding on a disc with 15 μm diamond. Then the samples were mechanically polished (final stage 1 μm diamond). After each preparation step the samples were ultrasonically cleaned in ethanol.

For the determination of carbon by EPMA the samples were subjected to a final polish with 0.05 μm γ-Al_2O_3 and then rinsed with demineralized water and finally cleaned ultrasonically in ethanol.

The as-prepared TiC_x/Fe–C specimens were mounted in the X-ray diffractometer without further preparation. For the X-ray diffractometry of both sides of a coating, from each specimen series (see Section 2.2) a TiC_x coating was detached from the substrate in the following way. From the CVD specimen a disc-shaped sample of 30 mm diameter and 1 mm thick was cut with a diamond saw. The disc was moulded in a cold-mounting compound (Technovit 3040, Kulzer, FRG). The substrate was removed by grinding on SiC emery paper and finally by etching in a solution of 8 wt % HCl in water at about 330 K. The remaining chips of the TiC_x coating were rinsed in demineralized water and the mould was removed in chloroform. Finally the TiC_x coating was mounted on a (510) oriented silicon single crystal wafer (48 mm diameter and 1 mm thick) using grease (Glisseal, Borer Chemie, Switzerland).

3. Methods of investigation

3.1. Metallography

Light microscopy of the cross-section was performed with a Neophot-2 microscope (Carl Zeiss, Jena, GDR). By etching in a 2% nital solution (see Section 2.3) the grain boundaries and phase boundaries of the Fe–C substrate were preferentially attacked, whereas the TiC_x coating remained unattacked.

The microhardness was determined on cross-sections as a function of the distance to the coating/substrate

interface using a Vickers microhardness tester according to Hanemann, adapted to the Neophot-2 microscope (applied load: 6.4 g). The diagonals of the hardness indentations were measured in differential interference contrast. Interference by neighbouring indentations or surfaces/interfaces was avoided by maintaining a sufficient distance [11].

The scales of the measuring oculars used for measuring thickness and microhardness were calibrated against an object of well-known length (10.0 μm). Each coating thickness and microhardness value presented was the mean of ten measurements.

Compo images and Fe$K\alpha$ and Cr$K\alpha$ images were made using a Jeol superprobe 733 (see Section 3.2).

3.2. Electron probe microanalysis

Electron probe microanalyses (EPMA) were performed with a Jeol superprobe 733 equipped with four wavelength-dispersive spectrometers and a fully automated analysis system (Tracor Northern).

To be able to perform simultaneous measurements of Ti$K\alpha$, C$K\alpha$, Cr$K\alpha$ and Fe$K\alpha$ the accelerating voltage had to be a compromise: 10 kV. Usually a beam current of 100 nA was applied. For titanium, chromium and iron, the pure element, and for carbon, Fe_3C, was used as a standard.

In the quantitative determination of first-order Ti$K\alpha$ radiation dead-time and pulse-shift problems were sometimes encountered. This was overcome by measuring second-order Ti$K\alpha$ radiation. The problems connected with the quantitative analysis of the light element carbon were dealt with according to Bastin and co-workers [12, 13].

3.3. Micro Auger electron spectroscopy

Auger electron spectroscopical (AES) analyses were performed with a PHI Multiprobe 600. To locate small second-phase particles in the TiC_x coatings with the scanning electron microscopy option, a rather high tension of 10 or 15 kV was required. Therefore, analyses of second-phase particles and of the coatings themselves were performed with the same high tension. A beam current of 5 or 10 nA was applied. Depending on the high tension and beam current, the beam size was between 100 and 300 nm during the AES analyses. The Auger electron spectra were automatically processed using data from Davis *et al.* [14].

3.4. X-ray diffractometry

3.4.1. Measurement procedures

X-ray diffraction measurements were performed with a Siemens ω-diffractometer (type D500) equipped with a curved graphite monochromator in the diffracted beam and using Cu$K\alpha$ radiation. During measurements the specimen was rotated around the surface normal. The temperature was controlled to within ± 0.5 K.

For phase identification, diffractograms were recorded from 30 to 100° 2θ with 0.05 or 0.1° 2θ step size and 40 sec counting time per step.

For the determination of the strain-free lattice parameter (see Section 3.4.2) and for line-profile analysis (see Section 3.4.3) the TiC_x 422-Cu$K\alpha$ reflection was chosen because it nicely combines (i) a minimal overlap with adjacent reflections, and (ii) a large 2θ value to obtain a high accuracy in the determination of the lattice spacings and a large specimen tilt (see Section 3.4.2) in the ω diffractometer.

The measured profiles were corrected for (i) the dead time of the counting system, (ii) a linear background fitted to the extremities of the profile recorded, (iii) the angle-dependencies of Lorentz-polarization [15] and absorption factors, and (iv) the presence of $K\alpha_2$ radiation [16]. Thereafter, the peak positions were determined by fitting a parabola to the peak region of the profiles. Systematic (small) errors in the peak positions, due to defocussing (increasing with increasing ψ), were eliminated by calibration against a stress-free TiC reference sample (see below) which was calibrated against a well-defined silicon powder (NBS SRM 640 [17]). From the peak positions thus found, the lattice spacings were calculated.

In the line-profile analysis, for the elimination of the broadening due to the instrumental aberrations and the X-ray spectrum the 422-Cu$K\alpha$ reflection was measured from the TiC reference sample mentioned. This sample consists of a TiC powder (Starck, FRG) annealed at 1470 K for 260 h in a sealed quartz tube filled with argon.

3.4.2. Determination of strain-free lattice parameters

To determine the composition of solid solutions from lattice parameters, one has to account for internal stresses (strains): the lattice parameter has to be calculated from strain-free lattice spacings. These can be determined by use of the so-called $\sin^2\psi$-method for the X-ray diffraction determination of stresses [18].

For the specimens investigated, it was experimentally verified that the stresses parallel to the sample surface are equal for all directions in the surface [10]. Then the following relation holds

$$\frac{d_\psi - d_0}{d_0} = 2s_1^{hkl}\sigma_\parallel + \tfrac{1}{2}s_2^{hkl}\sigma_\parallel \sin^2\psi \qquad (1)$$

where $h\,k\,l$ denote the indices of the diffracting lattice planes, ψ is the angle between the normal to the specimen surface and the normal to the diffracting lattice planes, d is the $h\,k\,l$ lattice spacing, d_0 is the strain-free $h\,k\,l$ lattice spacing, s_1 and $\frac{1}{2}s_2$ are the X-ray elastic constants for the $h\,k\,l$ planes and $\sigma_\parallel$ is the stress parallel to the coating surface.

For the TiC_x coatings investigated, always a linear relation between d_ψ and $\sin^2\psi$ was found [10] in accordance with Equation 1.

The strain-free lattice spacing, d_0, has been obtained from a plot of d_ψ against $\sin^2\psi$. From Equation 1 it follows (for the state of stress considered) that d_0 is found at

$$\sin^2\psi_0 = \frac{-2s_1^{hkl}}{\frac{1}{2}s_2^{hkl}} \qquad (2)$$

where ψ_0 is the strain-free direction. The X-ray elastic constants s_1 and $\frac{1}{2}s_2$ were calculated (cf. [10]) from the single-crystal elastic constants of $TiC_{0.91}$ [19] by using the Eshelby–Kröner model [20]. The strain-free direction thus found was verified experimentally [21].

3.4.3. Line-profile analysis

The broadening of observed X-ray diffraction lines is caused by the imperfection of the microstructure of the specimen, instrumental effects and the X-ray spectrum used. The imperfection of the microstructure as deduced from the line broadening is commonly expressed in terms of crystallite size, D, and microstrain, e [22]. Lattice imperfections as misfitting particles, dislocations and dissolved atoms, cause local distortions of the lattice and therefore contribute particularly to the microstrain.

For much of the discussion in Section 4.2.3 it suffices to realize that an observed diffraction line is the broader the more imperfect is the microstructure. For quantitative line profile analysis, the broadening due to the instrument and the X-ray spectrum used has to be removed by use of a reference specimen. In the case where the reference specimen has an imperfect microstructure (crystallite size D_r and microstrain e_r) and the single-line Voigt method [23] is applied, relative measures D_m and e_m for size and strain, respectively, are obtained: $D_m^{-1} = D^{-1} - D_r^{-1}$ and $e_m^2 = e^2 - e_r^2$. On this basis the difference in microstructure was studied of the free-surface and substrate regions of coatings detached from their substrate (see Section 2.3).

4. Results and discussion

4.1. Chemical constitution of substrates and coatings

In all coating/substrate combinations investigated, small amounts of the elements oxygen, chlorine, chromium and iron were present (the composition of the substrates before coating is described in Section 2.1). The amounts of oxygen and chlorine were insignificant (< 0.5 at %) as compared to the amounts of chromium and iron (see Table I). A typical example of the composition as a function of distance in the coatings and Fe–C substrates is shown in Fig. 1. Similar composition profiles were obtained for the other coating/substrate combinations. In the following sections, a detailed discussion will be given of the chemical constitution of the coatings and substrates with respect to chromium, iron, titanium and carbon.

4.1.1. Chromium

The chromium content of the TiC_x coatings and of the substrate regions adjacent to the coatings of specimen series A, B and C (see Section 2.2) decreased in the order A, B, C (see Table I). In addition, it was found for each specimen series that in the coating of the substrate with 0.27 wt % C the chromium content was lower than in the coatings on the other substrates with higher carbon content.

The chromium originates from the reactor environment. The reactor system employed (see Section 2.2) is commonly used in the industry for coating of tool steels with TiC_x. The tool steels and also the reactor vessel contain chromium. Probably the chromium incorporated in the TiC_x coatings was transported during the CVD process to the specimens through the gas phase in the form of chloride(s). The concentration of the chloride(s) in the gas phase will depend on (i) the state of the reactor, (ii) the loading of the reactor, and (iii) the CVD process conditions. Apparently, conditions (i) and (ii) were different for specimen series A, B and C.

The chromium content of the substrates declines to zero at about 10 to 20 μm from the coating/substrate interface (see Fig. 1a). The amount of chromium in the substrates increases with increasing carbon content of the substrates. This must be due to the high affinity of chromium to carbon.

The chromium content of the TiC_x coatings is practically constant throughout the coating (Figs 1a and d). In the TiC_x coatings of specimen series A, there is a slight decrease of the chromium content towards the substrate (Fig. 1a).

4.1.2. Iron

For all the TiC_x coatings investigated, the iron content near the free surface is nearly the same (see Table I) and in a region near the substrate it increases (Fig. 1a). This region is much smaller for the coatings of series C than for the coatings of series A and B. The iron-rich region, which is clearly observed in the Fe$K\alpha$ images (Fig. 1c) corresponds to the region in the compo images where second-phase particles are observed (white dots in Fig. 1b).

The iron is probably incorporated in the TiC_x coatings in the same manner as chromium (see above). According to Rudolph and Schlamp [24] volatile iron chlorides can be formed, particularly in the beginning of the CVD process when the Fe–C substrates are not completely covered with TiC_x. As in the case of chromium, the iron content of the TiC_x coatings will depend on the state and loading of the reactor vessel and on the CVD process conditions. Also diffusion of iron from the substrates into the TiC_x coatings may have occurred.

4.1.3. Titanium

There is a sharp interface between the TiC_x coatings and the Fe–C substrates (cf. Figs 2a and b). This is also reflected by EPMA (Fig. 1) and by AES (Figs 2c and d). The titanium is almost constant in the TiC_x coatings and is practically zero in the substrates. Thus no diffusion of titanium into the substrates has occurred during the CVD process. It is also observed that the titanium content of the coating is relatively low if the chromium content is high: chromium seems to replace titanium (see Section 4.2.2).

4.1.4. Carbon

The carbon content of the substrate changes with the distance to the coating/substrate interface (Fig. 1): near the coating the carbon content is higher than in the bulk of the substrate, then it declines (as the chromium content does) to a value below the carbon content of the bulk of the substrate. After a carbon-depleted zone, the carbon content increases to the carbon content of the bulk of the substrate.

The growth rate of the TiC_x coatings is mainly determined by the carbon content of the substrates and to a lesser extent by the presence of CH_4 in the gas phase during CVD [25]. The carbon content of the

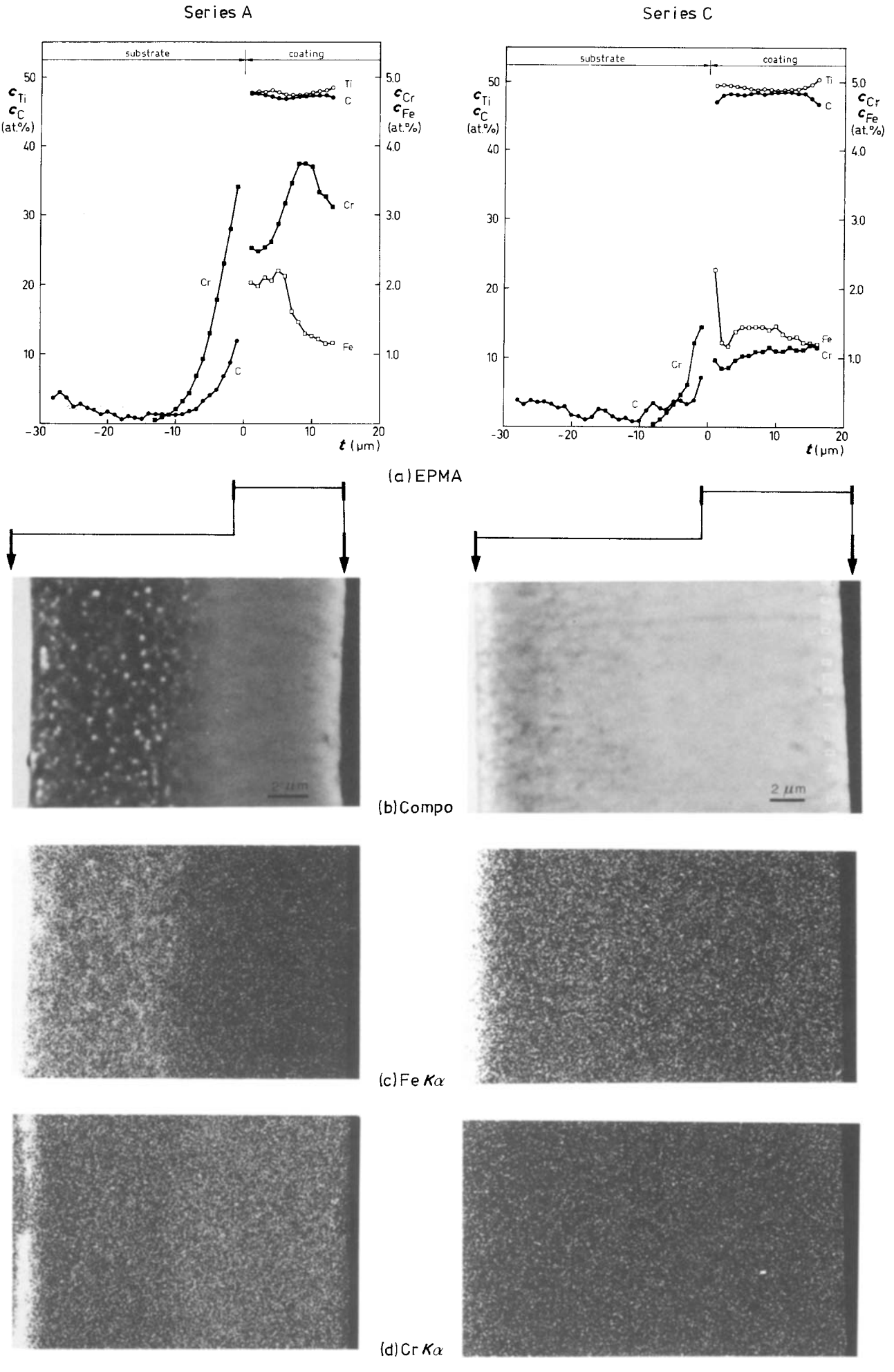

Figure 1 Composition, c, as a function of distance, t, to the coating/substrate interface of CVD TiC_x coatings on Fe–C substrates with 3.4 at. % C (0.76 wt % C). Specimen series A and C. Results obtained by EPMA.

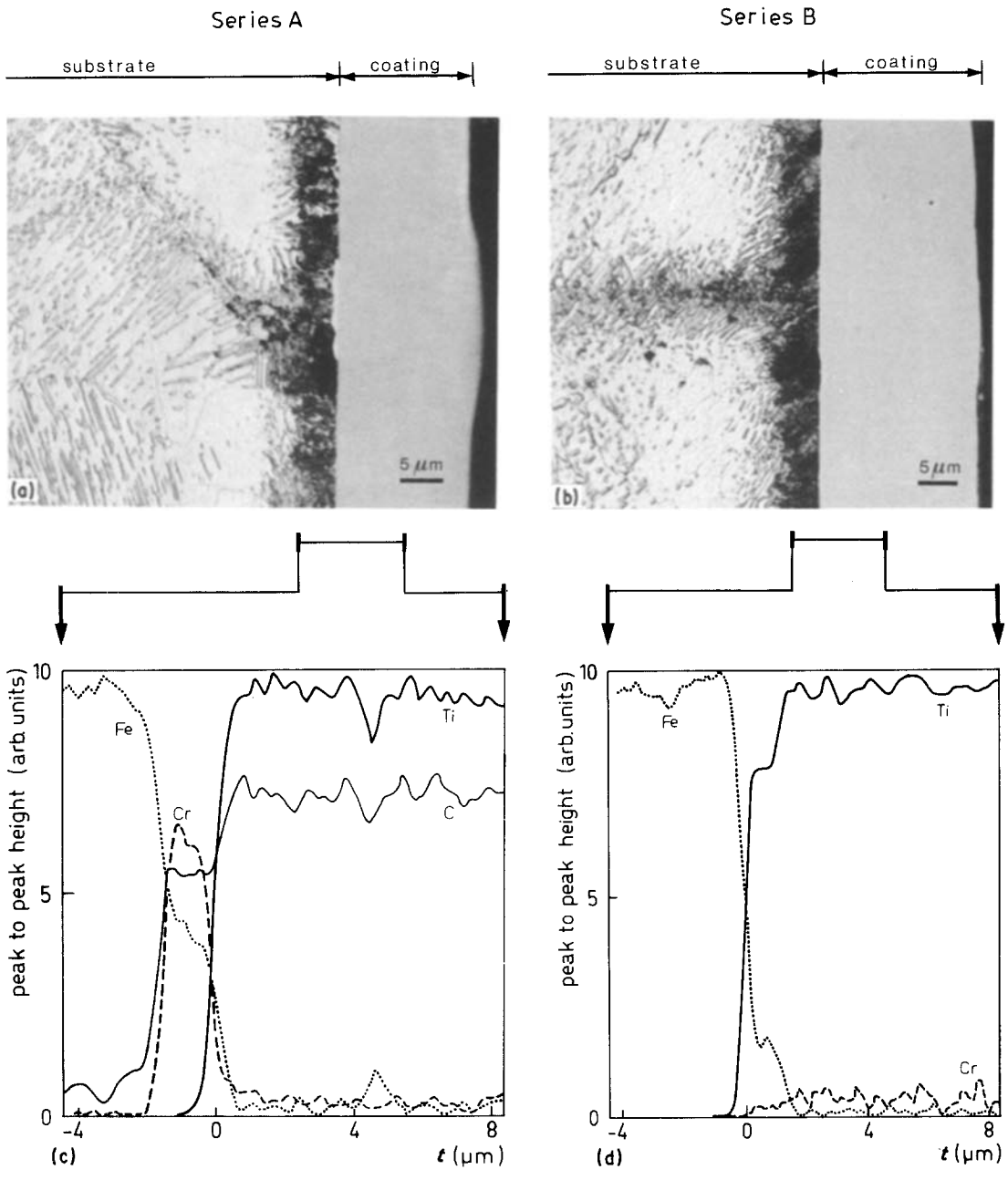

Figure 2 (a), (b) Light microscopical images of cross-sections of CVD TiC_x coatings on Fe–C substrates with 3.4 at. %C (0.76 wt % C). (c), (d) AES line scans across the CVD coating/substrate interface.

coatings, however, appears to be almost independent (see Table I) of both the carbon content of the substrates and the presence of CH_4 during CVD (see also Section 4.1.7).

4.1.5. The substrates, effects of chromium

The chromium present in the substrate region adjacent to the TiC_x coatings influences the microstructure of the substrate and the growth kinetics of the coating. Figs 2a and b show that in the substrates, starting from the coating/substrate interface, a small zone is present with a fine lamellar structure of ferrite and carbide, which is followed by a carbide-depleted zone. This is explained as follows. (i) The chromium concentration profile as measured (see Fig. 1a) exists already at the CVD temperature (1273 K), because the diffusion rate of chromium in austenite is relatively small. Because chromium decreases the carbon activity in austenite [26], carbon segregates to this chromium-rich region (see Fig. 1a). (ii) On cooling from the CVD temperature to room temperature, the austenite decomposes into ferrite and a carbide. With chromium present, it concerns an Fe,Cr-carbide (M_3C of M_7C_3 [27]). The temperature at which, on cooling, the Fe, Cr-carbide begins to form increases with increasing chromium content [26]. The formation of ferrite and Fe,Cr-carbide begins at the coating/substrate interface where the chromium content is highest. This gives rise to long-range diffusion of carbon resulting again in an increase of the carbon content in the region where chromium is present in the substrate (see Fig. 1a). On further cooling, ferrite and cementite are formed (at $\sim$ 1000 K) in the bulk of the Fe–C substrates. Both the diffusion of carbon to the chromium-rich zone and the formation of cementite in the bulk of the substrate, result in a carbide-depleted zone (see Fig. 1a).

In coated substrates with a relatively high chromium content (series A) the original austenite grain

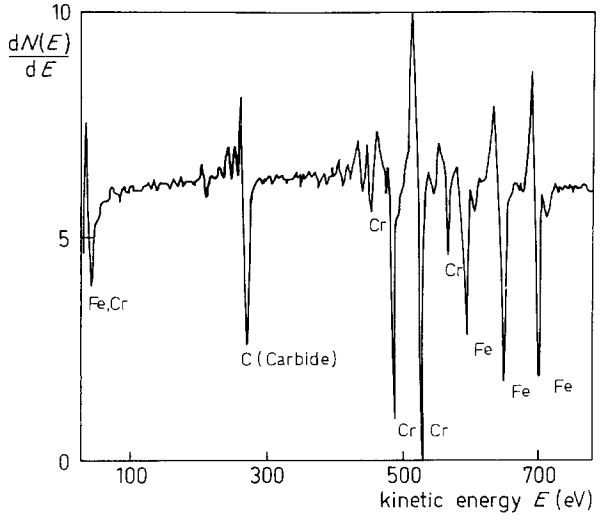

Figure 3 AES point analysis at interlayer of CVD TiC_x coating on Fe–C substrate with 3.4 at. % C (0.76 wt % C). Specimen series A (see Figs 4a and c). Auger spectrum in the differential distribution.

boundaries are decorated with a fine lamellar structure of ferrite and an Fe,Cr-carbide (Fig. 2a) or with a pro-eutectoid Fe,Cr-carbide in the case of substrates containing ≥ 0.76 wt % C. Following a reasoning similar to that above, this is explained by a relatively fast diffusion of chromium along the grain boundaries during the CVD process.

In cases with a very high chromium content even a closed interlayer between coating and substrate is formed (cf. Figs 2a and c). An AES point analysis (Fig. 3) proves that this layer consists of an Fe,Cr-carbide.

Stresses in coating and substrate develop during cooling from the deposition temperature (1273 K) to room temperature. The absolute values of the strains measured are smaller than those expected from the differences in thermal shrink between coating and substrate. This is quantitatively explained by a full stress relaxation during the phase transformations occurring in the substrates on cooling [10]. However, in those cases where a pro-eutectoid Fe,Cr-carbide was formed at the original austenite grain boundaries in the substrate (see above), the absolute value of the strain measured was somewhat larger than that calculated. Obviously, the Fe,Cr-carbide particles hinder a full relaxation of stresses during the phase transformations in the Fe–C substrate.

4.1.6. The coatings, presence of iron, effects of chromium and iron

AES and XRD analyses were applied to reveal the nature of the second-phase particles in the region of the TiC_x coatings adjacent to the substrates (cf. Fig. 1b).

AES point analysis of the second-phase particles and of the TiC_x matrix (Figs 4a and b) and AES line scans (Fig. 4c) strongly indicate that these particles are iron-rich (because the particles are very small (~ 500 nm), the TiC_x matrix also contributes to the AES signal of a second-phase particle).

X-ray diffractograms (Fig. 5) of the substrate-side of TiC_x coatings detached from their substrates (see Section 2.3) show unambiguously that the second-phase particles consist of austenite and ferrite (see Section 4.2.2). In coatings with a high chromium content (~ 3.2 at. % Cr) only austenite is present.

This shows that not all the iron is in solid solution in TiC_x, in any case not in the region adjacent to the substrate. This agrees with the ternary phase diagram of Ti–Fe–C at 1273 K [28]. The fact that mainly

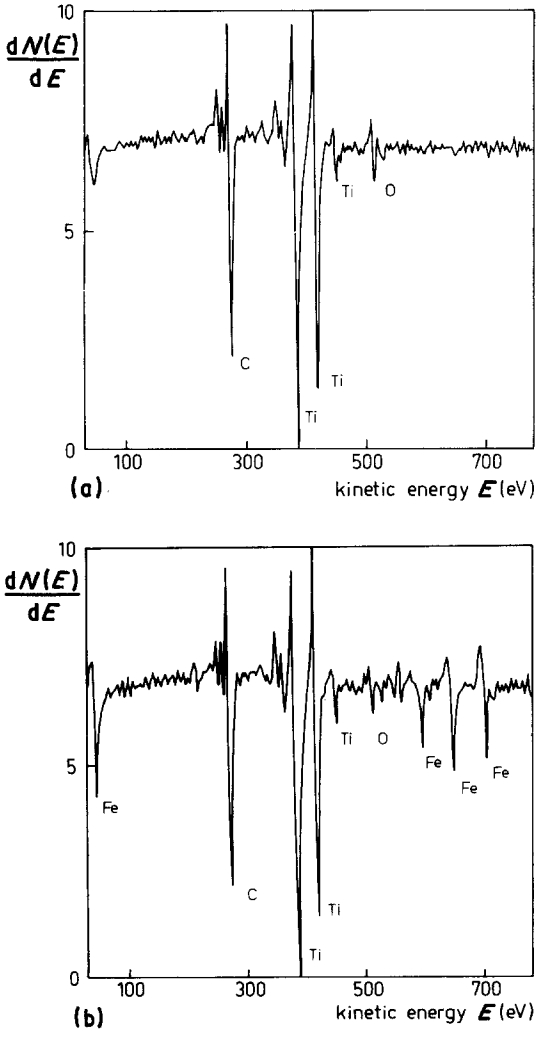

Figure 4 AES analyses of CVD TiC_x coating on Fe–C substrate with 3.4 at. % C (0.76 wt % C). Specimen series B. Auger spectra in the differential distribution. (a) Point analysis in the matrix of the coating. (b) Point analysis of a second-phase particle in the coating. (c) Fe line scan across a second-phase particle in the coating.

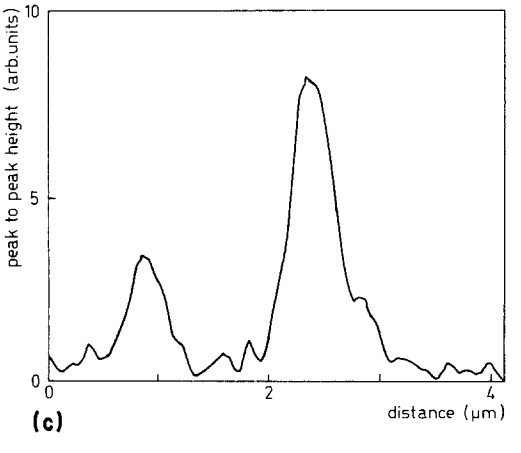

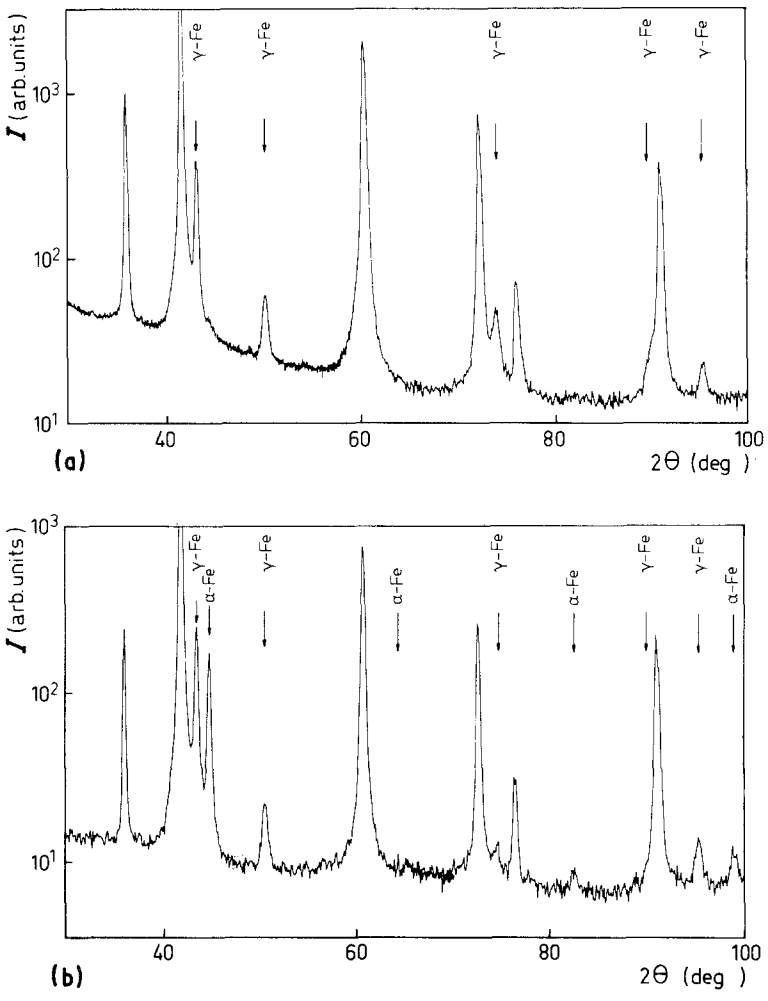

Figure 5 Diffracted Cu$K\alpha$ intensity I plotted against diffraction angle 2θ of the substrate side of CVD TiC_x coatings detached from their substrates. Ferrite (α-Fe) and austenite (γ-Fe) peaks are indicated. All other peaks are from TiC_x. (a) TiC_x coating with a high chromium content (3.2 at. % Cr). Specimen series A, substrate with 2.2 at. % C (0.48 wt % C). (b) TiC_x coating with a low chromium content (1.2 at. % Cr). Specimen series C, substrate with 3.4 at. % C (0.76 wt % C).

austenite is present, indicates that the iron particles were already present at the CVD temperature and did not form by a precipitation process during cooling after the CVD. Normally one would expect that austenite transforms to ferrite on cooling to room temperature. However, the presence of chromium may have hindered the transformation, as is also known for steels alloyed with chromium [29, 30].

The growth rates of the coatings of specimen series A, B and C increase in the order A, B, C (Fig. 6). It is also noted that the chromium contents of coatings and substrates decrease in the same order. This is explained as follows. The growth rate of CVD TiC_x on Fe–C substrates was found to be strongly dependent on the diffusion of carbon in the substrates [24] (see, however, also Section 4.1.7). In this context, the effect of CH_4 in the gas phase during CVD can be neglected [24]. Because the diffusion coefficient of carbon in austenite strongly decreases with increasing chromium content [31, 32], growth rates of TiC_x coatings on Fe–C substrates will decrease with increasing chromium content of the substrates.

No conclusive evidence about the effects of the second-phase iron particles on the growth rate of the TiC_x coatings is available. On the one hand the particles, and their surrounding strain fields (see Section 4.2.3), hinder the diffusion of carbon through the TiC_x matrix, on the other hand the diffusion of carbon in the iron particles is fast as compared to the diffusion of carbon in TiC_x.

4.1.7. The coatings, carbon to metal ratio, x

For series A and B the carbon content of the coatings as measured (see Fig. 1a) is almost constant throughout the thickness, whereas for series C the carbon content as measured decreases slightly with increasing distance to the coating/substrate interface (Fig. 1a). The carbon content near the free surface is about the same for all coatings investigated (46 to 47 at % C, see Table I).

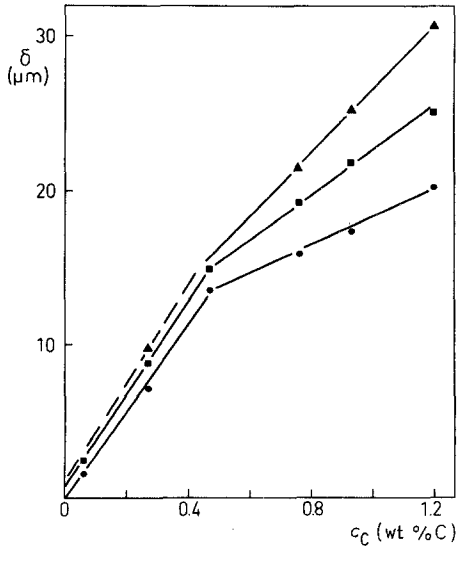

Figure 6 TiC_x coating thickness, δ, after 5 h CVD as a function of the carbon content of the Fe–C substrate, c_C. (●) Series A, (■) series B, (▲) series C.

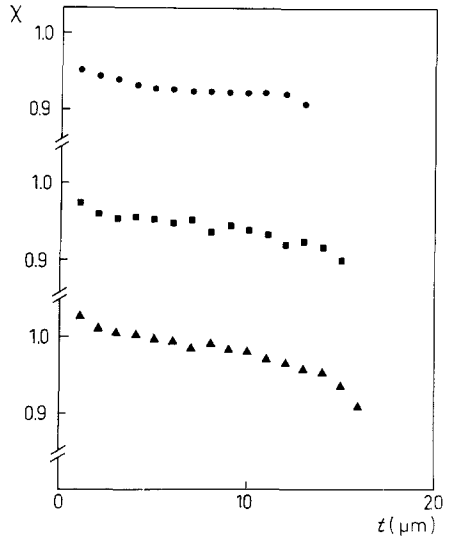

Figure 7 Carbon to metal ratio, x, as a function of distance, t, to the coating/substrate interface of CVD TiC_x coatings on Fe–C substrates with 3.4 at. % C (0.76 wt % C); see Equation 3. (●) Series A, (■) series B, (▲) series C.

Because the coatings do not consist of a single phase (see Section 4.1.6), the carbon content of the coatings as measured by EPMA does not give direct information about the chemical composition of the carbide formed by the CVD process. In Section 4.2.2 evidence is given that in the coatings of all series all the chromium present is in solid solution in the TiC_x. The situation for the iron is less simple: where the chromium content is high the iron is not in solid solution (within the limits of detection) and with a low chromium content (part of) the iron may be in solid solution.

In accordance with Section 4.2.1 and ignoring the presence of iron in the TiC_x lattice the carbon to metal ratio, x, is calculated from

$$x = \frac{\text{at \% C}}{\text{at \% Ti} + \text{at \% Cr}} \qquad (3)$$

The x values thus found are given as a function of distance to the coating/substrate interface in Fig. 7. The carbon to metal ratios for series C are somewhat higher than for series A and B, indicating that in the coatings of series C, who have a low chromium content (see Table I), some iron may be in solid solution in TiC_x (then the denominator of Equation 3 should be extended with the at % Fe in solution).

The present establishment of a gradient in the carbon to metal ratio of the TiC_x coating (Fig. 7) may be important in a further study of the kinetics of the growth of CVD TiC_x layers on Fe–C substrates. Although the TiC_x phase can exist over a wide composition range ($0.61 < x < 0.96$ [6]), the carbon to metal ratio of the TiC_x phase in the present investigation is roughly the same for all the coatings, namely $x \approx 0.9$. It was noted [25] that at this x the free energy of formation of pure TiC_x is minimal [33], the melting point exhibits a maximum [9] and the lattice parameter is maximal [3, 34]. Recently, Hauck [35] has given a theoretical explanation for this. However, the value of $x \approx 0.9$ may also stem from the present experimental CVD conditions, because Teyssandier *et al.* [36] have shown that x can be varied between 0.67 and 1 by merely varying the $TiCl_4$ and CH_4 partial pressures in the input gas phase.

4.2. Microstructure of the coatings

The effects of chromium and iron in particular on the microstructure of the TiC_x coatings will be discussed in terms of strain-free lattice parameter, lattice imperfections and microhardness.

4.2.1. Effect of oxygen, chromium and iron on the lattice parameter of TiC_x

The relation between the lattice parameter of pure TiC_x and the composition x has been given by Storms [34]. Literature data have been evaluated to estimate the influence of oxygen, chromium and iron on the lattice parameter of TiC_x; data about the influence of chlorine are not available, to our knowledge.

TiC_x has an NaCl structure. Density measurements and neutron diffraction indicate that departure from stoichiometry is due to vacancies on the carbon sites only [34]. Consequently, x is the fraction of carbon sites occupied.

TiO has also the NaCl structure and can form solid solutions with TiC_x at all compositions [37]. Chromium and iron have a limited solid solubility in TiC_x. At 1273 K the maximum solid solubility of chromium in TiC_x is about 2.0 at. % Cr according to Guha and Kolar [38] and the maximum solid solubility of iron in TiC_x is 1.3 ± 0.2 at. % Fe according to Ramaekers *et al.* [28].

The elements forming solid solutions with TiC_x will be divided into two types: Y and Z. Y stands for the elements which occupy carbon sites (like oxygen) and Z stands for the elements which occupy titanium sites (like chromium and iron). Let x be the fraction of carbon sites occupied, y the fraction of carbon sites occupied by Y atoms and z the fraction of titanium sites occupied by Z atoms. Then in $Ti_{1-z}Z_zC_{x-y}Y_y$:

$$\begin{aligned} x - y &= N_C/(N_{Ti} + N_Z) \\ y &= N_Y/(N_{Ti} + N_Z) \\ z &= N_Z/(N_{Ti} + N_Z) \\ 1 - x &= \text{fraction vacancies on carbon sites} \end{aligned} \qquad (4)$$

where N is the number of atoms of the element concerned.

It is assumed that:

(i) only small amounts of carbon and/or titanium are substituted by atoms of the concerning elements;

(ii) changes of lattice parameter due to the different elements are independent;

(iii) the change of lattice parameter per atomic fraction foreign element is independent of x.

The lattice parameter, a, of the solid solution can then be written as:

$$a = a_x + \sum_i y_i \left(\frac{\partial a}{\partial y}\right)_i + \sum_j z_j \left(\frac{\partial a}{\partial z}\right)_j \qquad (5)$$

where a is the lattice parameter of $Ti_{1-z}Z_zC_{x-y}Y_y$ and a_x is the lattice parameter of pure TiC_x (i.e. $y = 0$ and $z = 0$). The slopes $\partial a/\partial y$ and $\partial a/\partial z$ for, respectively, the elements oxygen, chromium and iron are derived from the literature and are summarized in Table II.

TABLE II Influence of oxygen ($\partial a/\partial y$), and of chromium and iron ($\partial a/\partial z$) on the lattice parameter of TiC_x (see Equation 5) as calculated from selected literature data

Element	$\frac{\partial a}{\partial y}$ or $\frac{\partial a}{\partial z}$ (10^{-3} nm)	Data source
O	7 ± 2	[39, 40]
Cr	22.5 ± 1.0	[40]
Fe	14 ± 3	[41]

4.2.2. Solubilities of chromium and iron from strain-free lattice parameter

The strain-free lattice parameter determined from the 422-Cu$K\alpha$ reflection of TiC_x is representative for the region near the free surface of the coating, because the information depth [21] is about 3 μm in the strain-free direction.

Assuming that all chromium and iron is in solid solution, the strain-free lattice parameter can be calculated using Equation 5 and using data from Table II. The carbon to metal ratio, x, at the free surface is in the range of 0.8 to 0.9 (see Fig. 7). In this composition range such large variations in x have only little influence on the strain-free lattice parameter of TiC_x [34]. One may take $a_x = 0.433\,13 \pm 0.000\,03$ nm. In the first instance the presence of oxygen and chlorine (see Table I) is not taken into account. The iron content is nearly the same for all coatings except one (1.2 ± 0.2 at. % Fe; $z_{Fe} = 0.022 \pm 0.004$; Table I) and the strain-free lattice parameter is lowered by $0.000\,31 \pm 0.000\,08$ nm. Because the chromium content is different for the TiC_x coatings investigated, Equation 5 eventually reduces to

$$a = (0.432\,82 \pm 0.000\,11) - (0.0225 \pm 0.0010)\,z_{Cr}\ \text{nm} \quad (6)$$

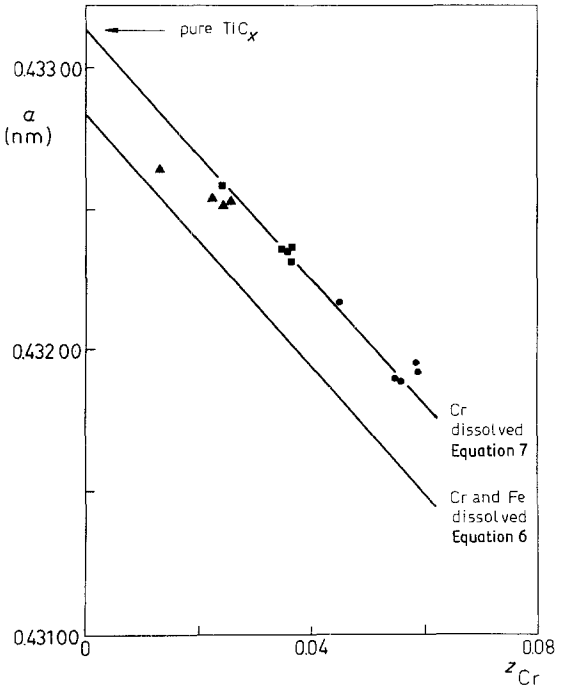

Figure 8 Strain-free lattice parameter, a, at the free surface of CVD TiC_x coatings on Fe–C substrates plotted against the chromium content, z_{Cr}, at the free surface (422-Cu$K\alpha$ reflection).

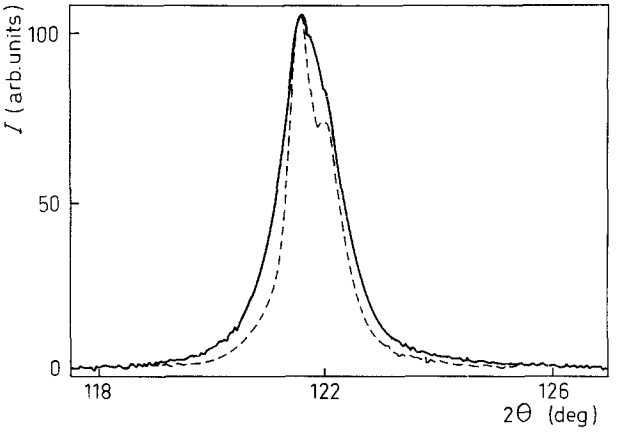

Figure 9 X-ray diffraction 422-Cu$K\alpha$ line profiles, (——) near the free surface, and (– – –) near the substrate, of a CVD TiC_x coating detached from the substrate. Specimen series C, substrate with 3.4 at. % C (0.76 wt % C).

As shown in Fig. 8 all strain-free lattice parameters measured are larger than those calculated using Equation 6.

It was shown that in the region of the TiC_x coatings near the substrate, iron is not in solid solution (see Section 4.1). Assuming that this is also the case in the region near the free surface, then

$$a = (0.433\,13 \pm 0.000\,03) - (0.0225 \pm 0.0010)\,z_{Cr}\ \text{nm} \quad (7)$$

This equation fits very well to the strain-free lattice parameters measured (see Fig. 8) which substantiates that:

(i) the chromium present in the TiC_x coatings is in solid solution, whereas the iron is not,

(ii) the iron is present as submicroscopic particles in the region of the coating near the free surface,

(iii) the influence of oxygen, chlorine and other possible impurities is not measurable.

Further, it follows from Fig. 8 and Equation 7 that the maximum solid solubility of chromium in TiC_x is at least 3.2 at. % Cr ($z_{Cr} = 0.058$) which contrasts with the value of 2.0 at. % Cr ($z_{Cr} = 0.036$) reported in the literature [38].

Finally, Fig. 8 shows that for low chromium contents, some iron can be in solid solution too: the strain-free lattice parameter for the TiC_x coating with the lowest chromium content calculated according to Equation 6 with $z_{Cr} = 0.013$ and $z_{Fe} = 0.015$ (see Table I, coating on substrate with 0.27 wt % C) agrees very well with the measured one.

4.2.3. Lattice imperfection

As a measure for the degree of lattice imperfection of the coatings, the integral breadths of the 422-Cu$K\alpha$ reflections (at $\psi = 0$) of TiC_x are used (see Section 3.4.1). For thick coatings (> 13 μm) detached from their substrates the integral breadth observed for the region near the free surface is considerably larger than for the region near the substrate; see Fig. 9. For these thick coatings the regions mentioned can be discriminated because of the absorption of the X-rays. The thinner coatings (< 9 μm) are not studied, because this discrimination proved to be less feasible. Fig. 10 shows

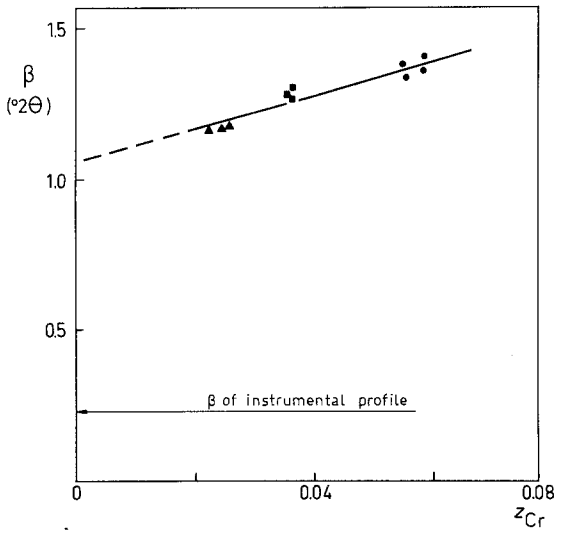

Figure 10 Integral breadth, β, of the X-ray diffraction 4 2 2-Cu$K\alpha$ line profile measured at the free surface of the CVD TiC_x coatings on Fe–C substrates plotted against the chromium content, z_{Cr}. (●) Series A, (■) series B, (▲) series C.

that the integral breadth observed for the region near the surface is large and that it increases slightly with the chromium content.

In the following paragraphs a discussion is given on the line broadening in relation to the formation and the microstructure of the TiC_x coatings investigated (see Section 3.4.3).

The broadening of the X-ray diffraction line profiles is found to be independent of internal (macro) stresses: no significant differences in integral breadths are observed before and after detaching the TiC_x coatings from their substrates, although the internal stress reduces from about 3000 MPa to approximately zero. A large lattice-spacing gradient (broadening the diffraction lines) due to a stress gradient is not expected in these TiC_x coatings [10]. In addition, the variation in the carbon to metal ratio, x, within the TiC_x coatings (see Fig. 7) will have little influence on the integral breadth, because the relative variation in lattice parameter caused by the variation of x is small ($\Delta a/a \approx 10^{-4}$, see Section 4.2.2).

The integral breadth observed for the region near the free surface of coatings with the same chromium content (i.e. the same specimen series, see Fig. 10) seems to be independent of the coating thickness (see Fig. 6) and, therefore, of the growth rate. This cannot be explained if selective growth of crystallites occurs during layer deposition: then crystallite size should increase and lattice distortion should decrease in line broadening with coating thickness.

According to Paulat *et al.* [42], for TiC_x coatings deposited on steels under conditions similar to those used here, a continuous nucleation with a high density occurs during growth. Their TEM investigations show a small grain size and no dislocations and stacking faults.

Line-profile analysis indeed shows that the broadening observed for the regions near the original substrate of the present TiC_x coatings is almost only caused by small crystallites: 30 to 40 nm. For the regions near the free surface the same crystallite size occurs, but in addition a microstrain of 1.6×10^{-3} is observed.

This additional microstrain broadening can be explained from the dispersion of the iron particles in the coatings. The microstrain in the TiC_x crystals caused by the iron particles increases with decreasing particle size because, with an almost constant volume fraction of iron throughout the coating (see Section 4.1), the total area of misfitting interface increases with decreasing particle size. The iron particles near the free surface are smaller than near the substrate. Therefore, the microstrain in the free-surface region is higher than in the near-substrate region. Apparently, the microstrain in the near-substrate region is too low to cause a measurable line broadening.

The small increase in integral breadth with the chromium content (Fig. 10) is probably caused by a microstrain originating from the dissolved chromium atoms in the TiC_x coatings. Fig. 10 suggests a linear relation between the integral breadth and the concentration of dissolved chromium atoms, the increase in microstrain is about 0.25×10^{-3} per at. % Cr.

4.3. Microhardness

Microhardnesses of TiC_x coatings with different chromium contents have been measured as a function of distance to the coating/substrate interface (see Fig. 11). The results for series A, B and C nearly coincide and the average value observed for the microhardness is only a little higher than reported for TiC_x with the same carbon to metal ratio, x [2–5].

As observed for the microstrain (see Section 4.2.3), the hardness of the coating also increases with increasing distance to the coating/substrate interface. Because the hardness indentations imply plastic deformation by slip [2, 42], the hardness will be influenced by the strain fields around the iron particles. For a material containing a volume fraction, f, of dispersed particles with radius, r, the hardening is proportional to $f^{3/2}r^{-1}$ [44]. Because the volume fraction of the iron particles in the TiC_x coating is approximately constant (see

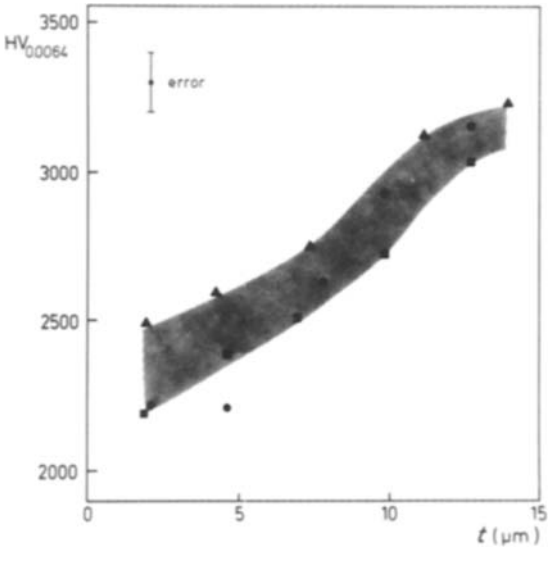

Figure 11 Microhardness, $HV_{0.0064}$, of the CVD TiC_x coatings as a function of distance, t, to the coating/substrate interface. (●) Series A, (■) series B, (▲) series C.

Section 4.1.2), it is expected that the hardness increases with decreasing particle size. This serves to explain why the hardness near the free surface of the coating is higher than near the coating/substrate interface. It is noted, however, that the hardness of TiC_x increases with increasing carbon to metal ratio, x [2–5]. In the present case x decreases slightly with increasing distance to the coating/substrate interface (Fig. 7) which suggests a decrease in microhardness in this direction. It is likely that both the carbon to metal ratio effect and the iron particle size effect occur, but the last effect seems to prevail.

As expected, the dissolution of chromium in the TiC_x coating has little effect on the value of the microhardness (Fig. 11), quite analogous to its effect on the microstrain (see Section 4.2.3). The high average value of the microhardness may be partially attributed to the small size of the TiC_x crystallites; no significant contribution is expected from dislocations or stacking faults, because their densities seem to be low (see Section 4.2.3).

5. Conclusions

Significant amounts of foreign elements are usually present in chemically vapour deposited coatings on steel substrates. The elements may originate from the equipment and the various workpieces in the reactor.

1. In the present TiC_x coatings on Fe–C substrates, chromium and iron are found. The chromium originates from the equipment, whereas the iron also stems from the substrates.

2. The Fe–C substrate region adjacent to the coating also contains chromium. It influences the microstructure of the substrate and thereby the carbon diffusion. The growth rate of the TiC_x coatings increases with increasing carbon content of the substrates and decreases with increasing chromium content of the substrates.

3. The chromium present in the coatings is in solid solution (up to 3.2 at. %). The effect of the chromium on the microstrain and hardness of the coatings is small.

4. The iron in the TiC_x coatings is present as small particles. The size of these particles decreases with increasing distance to the coating/substrate interface (from 500 nm to submicroscopic). The iron particles consist mainly of austenite in coatings with a high chromium content ($\sim$ 3 at. % Cr) and of austenite + ferrite in coatings with a low chromium content ($\sim$ 1 at. % Cr). The microstrain, as well as the hardness of the coatings, depends on the iron particle size and increases with increasing distance to the coating/substrate interface.

5. The carbon to metal ratio, x, of the TiC_x coatings is independent of the carbon content of the substrate. This ratio decreases with increasing distance to the coating/substrate interface.

6. The TiC_x crystallite size is 30 to 40 nm and constant throughout the thickness of the coatings. This small crystallite size probably contributes to the high hardness of the TiC_x coatings.

Acknowledgements

We wish to thank Ir M. M. Michorius and Mr G. Verspui of Philips Centre for Manufacturing Technology, Eindhoven, The Netherlands, for coating the substrates. We are obliged to Dr M. Weiss (Perkin-Elmer, Physical Electronics Division Europe, Munich, Federal Republic of Germany) for Auger analyses, to Mr D. P. Nelemans for electron probe micro-analyses and to Mr P. F. Colijn for skilful experimental assistance with the metallographic analyses. We also thank Dr F. J. J. van Loo for helpful discussions. Financial support from the "Stichting voor Fundamenteel Onderzoek der Materie" (Foundation for Fundamental Research of Matter) is gratefully acknowledged.

References

1. E. BROSZEIT and H. M. GABRIEL, *Z. Werkstofftechn.* **11** (1980) 31.
2. W. S. WILLIAMS, in "Propriétés Thermodynamiques, Physiques et Structurales des Dérivés Semi-métalliques" (Editions du Centre National de la Recherche Scientifique, Paris, 1967) p. 181.
3. L. RAMQVIST, *Jernkont. Ann.* **152** (1968) 517.
4. J.-L. CHERMANT, P. DELAVIGNETTE and A. DESCHANVERS, *J. Less-Common Metals* **21** (1970) 89.
5. G. V. SAMSONOV, M. S. KOVALCHENKO, V. V. DZWEMLINSKII and G. S. UPADYAYA, *Phys. Status Solidi (a)* **1** (1970) 327.
6. S. SARIN, *J. Appl. Phys.* **39** (1968) 3305.
7. D. L. KOHLSTEDT, W. S. WILLIAMS and J. B. WOODHOUSE, *ibid.* **41** (1970) 4476.
8. W. S. WILLIAMS, *Phys. Rev. A* **135** (1964) 505.
9. J. L. MURRAY, in "Binary Alloy Phase Diagrams", Vol. 1, edited by T. B. Massalski *et al.* (American Society of Metals, Metals Park, Ohio, 1986) p. 593.
10. W. G. SLOOF, R. DELHEZ, Th. H. de KEIJSER and E. J. MITTEMEIJER, *J. Mater. Sci.* **22** (1987) 1701.
11. M. SCHWARTZ, in "Deposition Technologies for Films and Coating", edited by R. F. Bunshah (Noyes, Park Ridge, New Jersey, 1982) p. 441.
12. P. P. J. RAMAEKERS, G. F. BASTIN, W. B. SLOOF, Th. H. de KEIJSER and R. DELHEZ, *Vacuum* **36** (1986) 19.
13. G. F. BASTIN and H. J. M. HEIJLIGERS, *X-ray Spect.* **15** (1986) 135.
14. L. E. DAVIS, N. C. MacDONALD, P. W. PALMBERG, G. E. RIACH and R. E. WEBER, in "Handbook of Auger Electron Spectroscopy", 2nd Edn (Physical Electronics Industries Inc., Eden Prairie, Minnesota, 1976).
15. R. DELHEZ, E. J. MITTEMEIJER, Th. H. de KEIJSER and H. C. F. ROZENDAAL, *J. Phys. E* **10** (1977) 784.
16. R. DELHEZ and E. J. MITTEMEIJER, *J. Appl. Crystallogr.* **8** (1975) 609.
17. C. R. HUBBARD, H. E. SWANSON and F. A. MAUER, *ibid.* **8** (1975) 45.
18. V. M. HAUK and E. MACHERAUCH, *Adv. X-ray Anal.* **27** (1983) 81.
19. R. CHANG and L. J. GRAHAM, *J. Appl. Phys.* **37** (1966) 3778.
20. F. BOLLENRATH, V. HAUK and E. H. MÜLLER, *Z. Metallkde* **58** (1967) 76.
21. W. G. SLOOF, M. A. J. SOMERS, R. DELHEZ, Th. H. de KEIJSER and E. J. MITTEMEIJER, in "Residual Stresses in Science and Technology", Vol. 1, edited by E. Macherauch and V. Hauck (Deutsche Gesellschaft für Metallkunde, Oberursel, 1987) p. 493.
22. R. DELHEZ, Th. H. de KEIJSER and E. J. MITTEMEIJER, *Fresenius Z. Anal. Chem.* **312** (1982) 1.
23. Th. H. de KEIJSER, J. I. LANGFORD, E. J. MITTEMEIJER and A. B. P. VOGELS, *J. Appl. Crystallogr.* **15** (1982) 308.
24. G. RUDOLPH and G. SCHLAMP, *Metalloberfläche* **23** (1970) 130.

25. P. P. J. RAMAEKERS, Thesis, University of Technology, Eindhoven (1985).
26. R. LUNDBERG, M. WALDSTRÖM and B. UHRENS, *CALPHAD* **1** (1977) 159.
27. W. D. FORGENG and W. D. FORGENG Jr, in "Metals Handbook", Vol. 3, edited by T. Lyman *et al.* (American Society for Metals, Metals Park, Ohio, 1973) p. 402.
28. P. P. J. RAMAEKERS, F. J. J. VAN LOO and G. F. BASTIN, *Z. Metallkde* **76** (1985) 245.
29. R. C. SHARMA, G. R. PURDY and J. S. KIRKALDY, *Metal. Trans.* **10A** (1979) 1129.
30. J. R. BRADLEY, G. J. SHIFLET and H. I. AARONSON, in "Proceedings of an International Conference on Solid → Solid Phase Transformations", Pittsburg, Pennsylvania, 1981, edited by H. I. Aaronson *et al.* (The Metallurgical Society of AIME, New York, 1982) p. 819.
31. J. KUCERA and K. STRANSKY, *Mater. Sci. Engng* **52** (1982) 1.
32. M. A. KRISHTAL, in "Diffusion Processes in Iron Alloys" (Keter Press, Jerusalem, 1970) p. 103.
33. F. TEYSSANDIER, M. DUCARROIR and C. BERNARD, *CALPHAD* **8** (1984) 406.
34. E. K. STORMS, in "The Refractory Carbides", Vol. 2 (Academic, New York, 1967) p. 8.
35. J. HAUCK, *J. Less-Common Metals* **105** (1985) 283.
36. F. TEYSSANDIER, C. BERNARD and M. DUCARROIR, in Proceedings of the 6th European Conference on Chemical Vapour Deposition, Jerusalem, March–April, 1987, edited by R. Porat (Iscar, Hardmetal Industrial Products, Nakaraya, Israel, 1987) p. 86.
37. G. NEUMANN, R. KIEFFER and P. ETTMAYER, *Monatsh. Chem.* **103** (1972) 1130.
38. J. P. GUHA and D. KOLAR, *J. Less-Common Metals* **31** (1973) 331.
39. Y. G. ZAINULIN, S. I. ALYAMOVSKY and G. P. SHVEIKIN, *J. Phys. Chem. Solids* **39** (1978) 29.
40. W. B. PEARSON, in "A Handbook of Lattice Spacings and Structures of Metals and Alloys", Vol. 1 (Pergamon, London, 1958) pp. 918, 961.
41. *Idem, ibid.*, Vol. 2 (1967) p. 1343.
42. E. PAULAT, P. LENK and G. WIEGHARDT, *Härterei Tech. Mit.* **39** (1984) 261.
43. D. J. ROWCLIFFE, in "Deformation of Ceramic Materials II", Material Science Research, Vol. 18, edited by R. E. Tressler and R. C. Bradt (Plenum, New York, 1984) p. 49.
44. N. J. GRANT, in "The Strengthening of Metals", edited by D. Peckner (Chapman and Hall, London, 1964) p. 163.

Received 26 May
and accepted 24 July 1987